

Possibility of observing Higgs bosons at the ILC in the lepton-specific 2HDM

Majid Hashemi*

*Physics Department, College of Sciences, Shiraz University,
Shiraz, 71946-84795, Iran*

The Higgs boson pair production at a linear e^+e^- collider is analyzed in the 4τ final state in the context of lepton-specific or type IV 2HDMs. Both beams are assumed to be unpolarized. The Higgs boson pairs (HA) are produced through off-shell Z^* production and decay to τ -jets which is the main decay channel for neutral Higgs bosons in 2HDM type IV. Using a simplified detector simulation based on the SiD detector at ILC, the 4τ signal is studied through the τ -jet pair invariant mass reconstruction. Several benchmark scenarios are considered for center of mass energies of 500 GeV and 1000 GeV at integrated luminosity of $500 fb^{-1}$. Among Standard Model (SM) background processes, the main background is $e^+e^- \rightarrow ZZ$ followed by $Z \rightarrow \tau\tau$. This background is however, well under control. With the luminosity assumed in the analysis, striking signals are obtained beyond the reach of LHC. Such signals would allow for precise determination of masses and cross sections and already much lower luminosities are sufficient for discovery.

I. INTRODUCTION

After the discovery of the Higgs boson at the LHC [1, 2] which was predicted through a theoretical framework known as the Higgs mechanism [3–8], attention has been paid to the question whether the observed particle belongs to a single $SU(2)$ doublet or is part of an extended structure such as a two Higgs doublet model (2HDM) [9–11]. Since the latter scenario can be made in a way to provide a light Higgs boson which respects the observed particle properties, one may expect an SM like structure consistent with experimental data plus new particles arising from the extended Higgs sector. Such additional Higgs particles can in general be different from the observed particle in terms of their masses and their couplings with SM fermions. Therefore one way to observe such particles would be to benefit from their characteristic features and decay channels which are different from those of the SM Higgs boson.

The additional Higgs bosons of such a model are assumed to be heavier than the observed one. Therefore, a center-of-mass energy above the threshold of their masses is required to observe them.

Obviously LHC is able to provide the effective center-of-mass energy required to produce heavy 2HDM Higgs bosons, however, in recent studies we have shown that the ability of linear colliders like ILC is much beyond LHC in observing their signals with a high statistical significance. In [12, 13] it was shown that signals from the type I 2HDM Higgs bosons can well be observed at e^+e^- colliders through $H/A \rightarrow b\bar{b}$. The leptonic decay of the type IV 2HDM Higgs bosons through $H/A \rightarrow \mu\mu$ was also shown to provide clear signals on top of the background [14, 15]. Results of the current analysis are also beyond the reach of LHC. The main reasons for such successful results can be summarized as follows.

First, the e^+e^- collisions provide a cleaner environ-

ment in terms of less particle multiplicity and hadron activity.

Second, some SM processes are simply absent in e^+e^- colliders because of the electric charge conservation. These processes include single W^\pm boson production and $W^\pm Z$ pair production.

Third, the SM background processes have a smaller cross section at e^+e^- colliders. As an example, while the top quark pair production, $t\bar{t}$, acquires a high cross section of $800 pb$ at LHC, it can appear through off-shell Z^* boson decay at e^+e^- colliders with a cross section of less than $1 pb$ at $\sqrt{s} = 500$ GeV.

The above arguments are not the only ones but can be considered as the main features which discriminate e^+e^- colliders from LHC.

A general 2HDM may be categorized into four CP-conserving types with different scenarios of Higgs-fermion couplings. The ratio of vacuum expectation values of the two Higgs doublets ($\tan\beta = v_2/v_1$) is the free parameter of the model and leads to enhancement or suppression of Higgs-fermion couplings compared to the corresponding SM couplings [16].

In total five physical Higgs bosons are predicted in 2HDM. The lightest Higgs boson, h , (sometimes denoted as h_{SM}) is assumed to be the SM-like Higgs boson with the same couplings with fermions as in SM. There are two heavier neutral Higgs bosons, H (CP-even) and A (CP-odd), and two charged Higgs bosons, H^\pm [17].

The search for the 2HDM Higgs bosons has been one of the main programs of high energy physics experiments since the time of LEP.

In what follows a brief review of the relevant experimental studies are presented. The relevance is in terms of either the 2HDM type IV or the final states involving $H/A \rightarrow \tau\tau$ decay.

One of the first analyses of the $\tau\tau$ final state is from DELPHI collaboration with $e^+e^- \rightarrow hZ$ and hA as the signal followed by $h/A \rightarrow b\bar{b}, \tau\tau$ at $\sqrt{s} = 189 - 208$ GeV. Their results were presented as limits on the branching ratio of the Higgs boson decay to $b\bar{b}$ and $\tau\tau$ [18].

The CDF collaboration reported analysis of $p\bar{p} \rightarrow HA$

* majid.hashemi@cern.ch

with $H/A \rightarrow \tau\tau$ using 1.8 fb^{-1} of integrated luminosity and excluded $\tan\beta > 50$ for a Higgs boson mass range $90 < m_A < 180 \text{ GeV}$ [19].

The D0 collaboration also published results of several studies. In a search for associated production of a Higgs boson and a b quark, followed by $H/A \rightarrow \tau\tau$, $\tan\beta > 30$ was excluded for $90 < m_A < 180 \text{ GeV}$ [20].

With more data using $H/A \rightarrow \tau\tau$ decays, the most stringent result of $p\bar{p}$ collisions was obtained by excluding $\tan\beta > 20$ for Higgs boson mass range $90 < m_A < 180 \text{ GeV}$ [21].

The CMS and ATLAS collaborations reported their analyses of $A \rightarrow Zh$ decay in the $\ell\bar{\ell}b\bar{b}$ final state based on $m_A = 300 \text{ GeV}$ assumption and presented exclusion contours for 2HDM types I and II (CMS) [22] and all four types (ATLAS) [23]. The lepton-specific 2HDM interpretation of the results by the ATLAS collaboration excluded $\tan\beta < 10$ [23]. One of the most recent analyses of all 2HDM types by the ATLAS collaboration has been presented based on a search for $A \rightarrow ZH$ decay at low $\tan\beta$ [24]. The $A \rightarrow ZH$ decay occurs when $m_A - m_H$ reaches the Z boson mass threshold and prefers low $\tan\beta$ because at high $\tan\beta$ the leptonic decay grows. The exclusion contours obtained in [24] are thus shown for $\tan\beta < 3$ and $m_A - m_H > 90 \text{ GeV}$.

The above reports are based on real data searches, while there are studies carried out for ILC and CLIC environment in the literature.

The Higgs boson program of the ILC begins at $\sqrt{s} = 250 \text{ GeV}$ which is near the peak of the cross section for $e^+e^- \rightarrow Zh$ [25]. One of the main operating scenarios of ILC is to perform e^+e^- collisions at $\sqrt{s} = 500 \text{ GeV}$ [26]. Ultimately, the ILC is upgradable to a center-of-mass energy of 1 TeV [25].

The Higgs physics at CLIC has also been extensively studied and presented in the CLIC conceptual design report [27–29]. In a recent review, a detailed study of different production processes and decay channels of the SM Higgs boson has been presented in [30].

The multi- τ final state of Higgs boson pair production has been shown to be a promising channel at LHC [31] and ILC [32]. Using a proper τ tagging algorithm, the four τ jets can be identified and used to reconstruct the Higgs bosons masses. There are enough kinematic constraints to reconstruct the two Higgs bosons with a high accuracy [32, 33]. This idea is used in the current analysis. The focus is on 2HDM type IV which allows for the heavy neutral Higgs boson decay to leptons while suppressing other decay channels. Since the τ lepton is the heaviest lepton, the decay to a τ pair is the dominant channel because the relevant Higgs-lepton couplings depend on the lepton mass. As Fig. 2 shows, at $\tan\beta = 3$, the Higgs bosons decay to $\tau\tau$ reaches $\sim 80\%$. Therefore below the top quark pair production threshold, $H/A \rightarrow \tau\tau$ is dominant, while above the threshold there is small reduction in the $H/A \rightarrow \tau\tau$ decay allowing $H/A \rightarrow t\bar{t}$ to appear at the level of a few percent. As seen from Fig. 1, $H/A \rightarrow t\bar{t}$ reaches 10% at high

masses leading to $\sim 10\%$ reduction of $H/A \rightarrow \tau\tau$ around $m_{H/A} \simeq 500 \text{ GeV}$. Since both neutral Higgs bosons (H and A) decay to τ lepton pairs, the signal process has a 4τ signature to be distinguished from SM background processes like $e^+e^- \rightarrow ZZ \rightarrow 4\tau$.

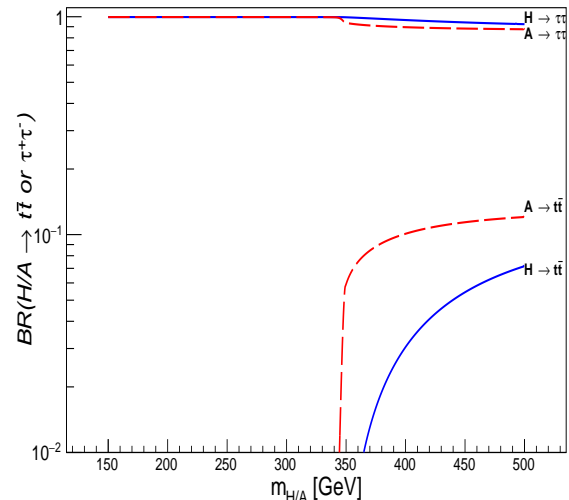


Figure 1. $BR(H/A \rightarrow XY)$ as a function of the Higgs bosons masses

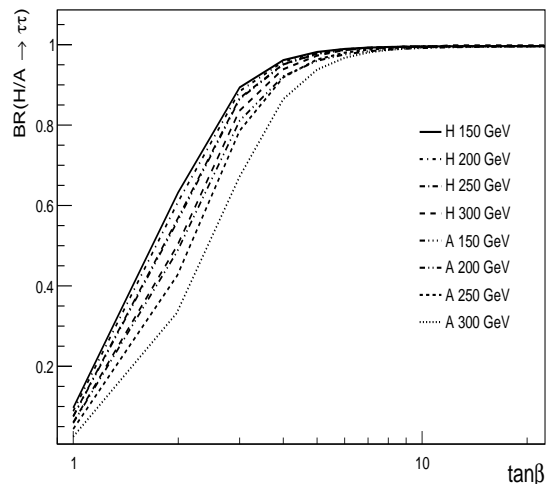


Figure 2. $BR(H/A \rightarrow XY)$ as a function of $\tan\beta$. The selected points showing H decays assume $m_A = 150, 250, 250, 300 \text{ GeV}$ from top to bottom. Similarly, points showing A decays assume $m_H = 150, 150, 250, 300 \text{ GeV}$.

The 2HDM type IV receives soft limits from flavour physics studies at low $\tan\beta$ [34–36]. Therefore the region of study is wide in $\tan\beta$ direction starting from values as low as $\tan\beta \simeq 1$ to 50. The signal process, i.e., $e^+e^- \rightarrow Z^{(*)} \rightarrow HA$ is independent of $\tan\beta$ as the ZHA vertex does not depend on Higgs-fermion couplings and

the 2HDM type. Therefore the signal process including Higgs bosons decays is effectively independent of $\tan\beta$. This is a dramatic feature of the signal under study as it makes it independent of any parameter other than the center of mass energy of the collider and the Higgs bosons masses. Therefore only kinematic effects can change the signal cross section and its observation chance.

The strategy of the analysis is to generate signal and background events and apply ILC detector simulation and perform τ identification algorithm using hadronic final state of τ leptons. The invariant mass of the two closest τ jets is then calculated and fills a distribution which serves as the Higgs boson candidate invariant mass. The same approach is applied on background events and a final assessment is made on the possibility of signal observation using statistical techniques. Before going to the details of the analysis, a brief review of the theoretical framework is presented in the next section.

II. THEORETICAL FRAMEWORK

The Higgs-fermion couplings in a general 2HDM appear as a Yukawa Lagrangian as in Eq. 1 [37].

$$\mathcal{L}_Y = \sum_{f=U,D,L} [\rho^f s_{\beta-\alpha} - \kappa^f c_{\beta-\alpha}] \bar{f} f H - i \sum_{f=U,D,L} \rho_A^f \bar{f} \gamma_5 f A \quad (1)$$

in which U, D, L are the up-type and down-type quarks and leptons fields, H and A the neutral Higgs boson fields, $\kappa^f = \frac{m_f}{v}$ are the SM Higgs-fermion couplings, $s_{\beta-\alpha} = \sin(\beta - \alpha)$ and $c_{\beta-\alpha} = \cos(\beta - \alpha)$. Here α is the neutral Higgs mixing angle.

The ρ^f parameters depend on the 2HDM type and are proportional to κ^f as shown in Tab. I specifically for type IV [38]. The CP-odd Higgs couplings (ρ_A^f) are the same as ρ^f except for an additional minus sign for $f = U$. Therefore the neutral CP-even Higgs couplings depend on the values of ρ^f which are κ^f (as in SM) times a $\tan\beta$ or $\cot\beta$ factor which leads to possible deviations from SM [39].

2HDM Type IV		
ρ^D	ρ^U	ρ^L
$\kappa^D \cot\beta$	$\kappa^U \cot\beta$	$-\kappa^L \tan\beta$

Table I. The type IV Higgs boson couplings with U (up-type quarks), D (down-type quarks) and L (leptons).

The light Higgs boson of 2HDM behaves the same as the SM Higgs by setting $s_{\beta-\alpha} = 1$ (the SM-like limit). This ensures the same couplings of the light Higgs with fermions and gauge bosons as in SM. Therefore one can assume that the observed particle is the light Higgs bo-

son of 2HDM. On the other hand, the above setting suppresses the heavy neutral CP-even Higgs coupling with gauge bosons which is proportional to $c_{\alpha-\beta}$ [17].

Under the assumption $s_{\beta-\alpha} = 1$, the brief form of the Lagrangian takes the form:

$$\mathcal{L}_Y = \sum_{f=U,D,L} \rho^f \bar{f} f H - i \sum_{f=U,D,L} \rho_A^f \bar{f} \gamma_5 f A \quad (2)$$

which is translated into the expanded explicit mode of Eq. 3 when Tab. I is used.

$$\mathcal{L}_Y = \frac{m^D}{v} \cot\beta \bar{D} D H + \frac{m^U}{v} \cot\beta \bar{U} U H - i \frac{m^D}{v} \cot\beta \bar{D} \gamma_5 D A + i \frac{m^U}{v} \cot\beta \bar{U} \gamma_5 U A + \frac{m^L}{v} \tan\beta \bar{L} L H - i \frac{m^L}{v} \tan\beta \bar{L} \gamma_5 L A \quad (3)$$

In such a scenario, Higgs boson conversion through $A \rightarrow ZH$ is also suppressed because at high $\tan\beta$ the leptonic decay dominates over the $\tan\beta$ independent $A \rightarrow ZH$ decay. Therefore both Higgs bosons, H and A , decay to τ pairs and the signal (invariant mass distribution of the two τ jets) contains τ jet pairs from both Higgs bosons.

It should be noted that a slight deviation from the SM-like limit (i.e., $s_{\beta-\alpha} \neq 1$) may drastically change the production and decay rates of the Higgs bosons [40].

The signal process in this analysis, i.e., $e^+e^- \rightarrow Z^* \rightarrow HA \rightarrow 4\tau$ depends on $s_{\beta-\alpha}$ through the $H.A.Z$ vertex and decreases if $s_{\beta-\alpha} \neq 1$. Under the same assumption, the fermionic decay $H/A \rightarrow \tau\tau$ decreases due to the possibility of $A \rightarrow Zh$ [22, 23], $H \rightarrow hh$ [41] and $H \rightarrow VV$ ($V = W, Z$) [42].

Detecting patterns of deviations in the SM-like Higgs boson coupling constants with precision data can fingerprint extended Higgs sectors. In a detailed study, expected precision of the Higgs boson coupling with gauge bosons has been obtained to be at the level of 4–6% at LHC high luminosity run at $\sqrt{s} = 14$ TeV and 0.39–0.49% at ILC operating at $\sqrt{s} = 500$ GeV [43]. The extended Higgs sectors can thus be indirectly tested by such precision measurements as the pattern of the deviations strongly depends on the structure of the Higgs sector (in this case, the type of 2HDM).

In the case of Higgs-gauge coupling, a precision measurement with 0.5 % uncertainty can be used to set upper limits on the value of α parameter as the Higgs-gauge coupling in 2HDM has an extra factor of $\sin(\beta - \alpha)$ compared to the corresponding coupling in SM. If it turns out that the coupling measurement is compatible with SM ($\sin(\beta - \alpha) = 1$) with 0.5 % uncertainty, then $0.99 < \sin(\beta - \alpha) < 1$ at 2σ (95% C.L.). For example, for $\tan\beta = 20$, this would leave an allowed region of $-0.05 < \alpha < 0.09$.

III. SIGNAL IDENTIFICATION AND THE SEARCH SCENARIO

The signal process is chosen to be $e^+e^- \rightarrow Z^{(*)} \rightarrow H A \rightarrow 4\tau$. Only the hadronic decay of the τ lepton is considered to benefit from the unique features of τ jets in the detector. The center of mass energy of the collider should be high enough to produce both Higgs bosons. Here two scenarios of $\sqrt{s} = 500$ and 1000 GeV are considered.

The analysis is based on two sets of benchmark points which are selected separately for each center-of-mass energy. Equal and different Higgs boson masses are included.

All benchmark points are consistent with the theoretical requirements including potential stability, perturbativity and unitarity as checked by using 2HDMC 1.7.0 [44, 45]. The selected points are also consistent with experimental limits according to HiggsBounds [46] and HiggsSignal [47] and results of all new references mentioned in the introduction.

For each selected point in the parameter space, an SLHA file [48, 49] (containing particles mass and decay spectrum) is provided by 2HDMC and is passed to PYTHIA 8.2.15 [50, 51] for event generation and cross section calculation.

Both beams are assumed to be unpolarized in the current analysis, although there are plans for polarized beam particles with polarization fraction of 80% (30%) for electrons (positrons) at $\sqrt{s} = 500$ GeV and 80% (20%) at $\sqrt{s} = 1000$ GeV [25].

In order to include initial state radiation (ISR) and the beam energy spectrum due to the effect of beamstrahlung, the event generation and detector simulation is performed in several steps. The hard scattering (the first few steps of each event before showering and hadronization) is performed by CompHEP [52, 53]. The beam parameters are given to CompHEP for each center of mass energy as shown in Tab. II [54]. The electron spectrum due to ISR has been calculated in [55]. In CompHEP a similar expression is used as obtained in [56, 57]. The effective energy spectrum of electron due to the effect of beamstrahlung is also simulated according to the function obtained in [58]. The net effect is a small reduction in the effective center of mass energy as seen in Fig. 3 which is obtained by calculating the incoming e^+e^- invariant mass, event by event, with or without ISR+beamstrahlung. The distributions shown in Fig. 3 are in good agreement with the official ILC results [59, 60]. The intrinsic beam spread is negligible compared to the ISR effect as shown in [60]. The final results are therefore marginally affected as seen in Fig. 4 for a reconstructed τ jet pair invariant mass distribution of the signal.

The output of CompHEP is stored in event files in LHA format [61] and is passed to PYTHIA for multi-particle interaction, final state showering and hadronization.

Events generated by PYTHIA are then used by DELPHES

3.4 [62] for detector simulation with a detector card specialized for SiD detector at ILC [63].

The jet reconstruction is performed by FASTJET 3.1 with inclusive k_t algorithm and jet cone size of 0.5 [64, 65]. The k_T algorithm has been found to give better performance by reducing the clustering of low p_T background in the forward/backward region [30]. The low p_T events of $\gamma\gamma \rightarrow$ hadrons are not simulated in this analysis. However, kinematic cuts $p_T > 5$ GeV and $15^\circ < \theta_\tau < 165^\circ$ are applied to all four jets in the event. Here θ_τ is the τ jet polar angle with respect to the beam axis.

A detailed study of $H \rightarrow \tau\tau$ and the beamstrahlung induced background from $\gamma\gamma$ and $e^\pm\gamma$ collisions shows that their contribution can be up to 50% of the SM background from direct e^+e^- interaction at $\sqrt{s} = 3$ TeV (CLIC) and 23% at $\sqrt{s} = 1.4$ TeV [30]. Such background processes are very important at high center of mass energies (CLIC environment) due to increasing number of beamstrahlung photons. The corresponding contribution at ILC environment is expected to be smaller. However, a detailed study is needed for a realistic estimation of this overlay background and could be subject of a future study which is probably beyond the scope of DELPHES capabilities and needs full simulation of the detector response.

Beam parameters	$\sqrt{s} = 500$ GeV, 1000 GeV	
No. of particles / bunch ($\times 10^{10}$)	2	1.74
RMS bunch length (mm)	0.3	0.225
RMS horizontal beam size (nm)	474	335
RMS vertical beam size (nm)	5.9	2.7

Table II. Beam parameters for beamstrahlung simulation taken from Tab. 8.2 of ILC technical design report volume 3 (Accelerator baseline) [54].

Tables III and IV show the selected points in the physical mass basis for the two center of mass energies of $\sqrt{s} = 500$ and 1000 GeV. The Higgs bosons are assumed to satisfy $m_A = m_{H^\pm}$ to ensure that deviation from SM in terms of $\Delta\rho$ is small enough and consistent with experimental value [66]. The selected points keep the Higgs bosons mass difference to be below the Z boson mass to suppress $A \rightarrow ZH$ decay. Table V shows the corresponding background cross sections at $\sqrt{s} = 500$ and 1000 GeV.

IV. SIGNAL SELECTION AND ANALYSIS

The DELPHES output is stored in ROOT files [67] which contain reconstructed physical objects like electrons, muons and jets with additional flags for b -tagging and τ -tagging results. The latter is what is used in the current analysis.

The event selection starts from accessing reconstructed jets which pass kinematic requirements mentioned ear-

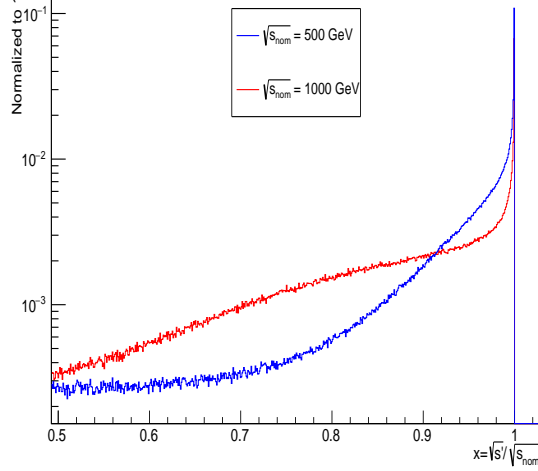


Figure 3. Distribution of the effective center of mass energy ($\sqrt{s'}$) including both beamstrahlung and ISR effects for the two cases of $\sqrt{s} = 500$ and 1000 GeV. $\sqrt{s_{\text{nom}}}$ is the nominal center of mass energy of the collider.

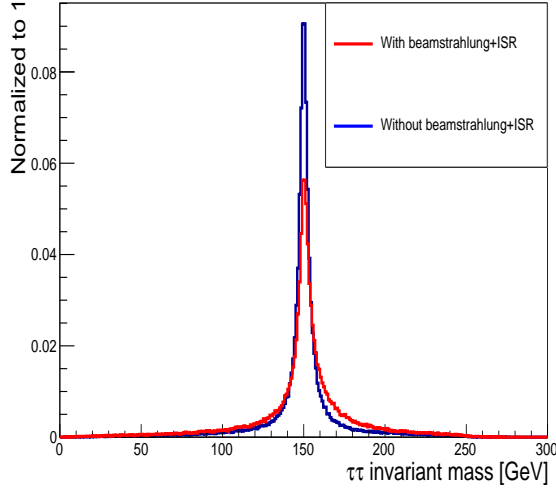


Figure 4. Signal of the τ -jet pair invariant mass at $\sqrt{s} = 500$ GeV with and without beamstrahlung+ISR.

lier. The τ -tagging is in general based on a sophisticated algorithm. The τ -jet should proceed in a narrow cone (isolated jet) accommodating one or three charged tracks associated with one prong or three prong hadronic decay with the hardest track carrying a large fraction of the jet energy. The τ -tagging algorithm which is used in this analysis relies on DELPHES implementation and is based on a simple matching method, where, the τ particle four-momentum is calculated from its decay products using generator level information. Then for every jet from the FASTJET output, a search is performed between all τ particles to find the closest τ to the jet under study. If ΔR

$\sqrt{s} = 500$ GeV				
	BP1	BP2	BP3	BP4
m_h	125			
m_H	150	150	200	200
m_A	150	200	200	250
$\tan \beta$	20			
σ [fb]	26.2	17.53	9.9	3.4

Table III. Signal benchmark points and their cross sections at $\sqrt{s} = 500$ GeV.

$\sqrt{s} = 1000$ GeV						
	BP1	BP2	BP3	BP4	BP5	BP6
m_h	125					
m_H	150	200	200	250	250	300
m_A	150	200	250	250	300	300
$\tan \beta$	20					
σ [fb]	12.2	10.3	9.2	8.3	7.2	6.3

Table IV. Signal benchmark points and their cross sections at $\sqrt{s} = 1000$ GeV.

Channel	Z/γ^*	ZZ	WW	$t\bar{t}$
$\sqrt{s} = 500$ GeV				
σ [fb]	16830	582	7855	598
$\sqrt{s} = 1000$ GeV				
σ [fb]	4318	234	3176	211

Table V. Considered background processes and their cross sections at $\sqrt{s} = 500$ and 1000 GeV.

between the τ -jet and the τ particle from generator level information is less than 0.2, the jet is identified as a τ -jet with an efficiency of 90% which is the case for $\tau \rightarrow \pi\nu$, $\rho\nu$ and $a_1\nu$ (3-prong decay) (see Tab. III-6.3 of ILC TDR [25]). Here ΔR is defined as $\Delta R = \sqrt{(\Delta\eta)^2 + (\Delta\phi)^2}$ with $\eta = -\ln \tan(\theta/2)$. The angles θ and ϕ follow the standard definitions: the polar and azimuthal angles.

The τ jet mistagging rate is also taken into account using the matching method with efficiency of 0.1%.

Events with at least four identified τ -jets are selected for the analysis. Requiring two τ -jets allows for a large background from single Z boson production.

For a reasonable event reconstruction, a τ four-momentum correction is performed [32, 33]. The idea is based on the fact that the number of momentum and energy conservation equations are equal to the number of scaling factors to be applied on the four τ jets in the

event. Therefore one can solve the four simultaneous equations (three for the total momentum conservation and one for the total energy conservation) and find the four unknown factors as in Eq. 4 (The unknown factors are z_1, z_2, z_3, z_4 and momentum/energy numerical indices denote the four τ jets $\tau_1, \tau_2, \tau_3, \tau_4$). This is of course based on the assumption that the τ jet direction has correctly been measured and a common factor can be applied to all its four-momentum components. This assumption is based on collinear approximation which implies that the visible τ jet and the associated neutrino are collinear in the high energy limit and the jet flight direction is approximately that of the τ lepton. Applying this correction, a dramatic improvement is obtained in the τ jet pair invariant mass distribution.

$$\begin{aligned}
z_1 p_1^x + z_2 p_2^x + z_3 p_3^x + z_4 p_4^x &= 0, \\
z_1 p_1^y + z_2 p_2^y + z_3 p_3^y + z_4 p_4^y &= 0, \\
z_1 p_1^z + z_2 p_2^z + z_3 p_3^z + z_4 p_4^z &= 0, \\
z_1 E_1 + z_2 E_2 + z_3 E_3 + z_4 E_4 &= \sqrt{s}
\end{aligned} \tag{4}$$

It should be noted that the four factors obtained in this way are required to be positive which is the case for most signal events but is useful to reduce the fake rate from SM background. When the τ jet four-momenta are rescaled, they are sorted in terms of the new energies and then the pairing is performed.

There are two ways to find the right τ -jet pairs from the Higgs bosons decays. One way is to find the τ -jet pair with minimum ΔR . This approach has shortcomings due to the fact that with increasing Higgs bosons masses, heavy Higgs bosons with sum of their masses being close to the center of mass energy, tend to be produced almost at rest in the laboratory frame and ΔR between their decay products tends to be large. Therefore the algorithm of finding the τ jet pair with minimum ΔR starts to be less efficient with increasing Higgs bosons masses.

Instead, the correct pairs of the τ jets are found by sorting them according to their energies and defining the two τ jets with maximum and minimum energies as one pair and the other two as the second pair. Therefore if τ jets are sorted in terms of their energies and labeled as $\tau_1, \tau_2, \tau_3, \tau_4$, the two pairs are made of τ_1, τ_4 and τ_2, τ_3 .

Each one of the above pairs may come from H or A . Therefore invariant mass distributions of both τ_1, τ_4 and τ_2, τ_3 pairs show the two Higgs bosons peaks if the Higgs bosons masses are different. This is a unique feature of this production channel.

Tables VI and VII show the signal and background selection efficiencies in the two scenarios of $\sqrt{s} = 500$ and 1000 GeV. No SM background other than ZZ survives at the end and the signal to background ratio is large in all cases. The high signal significance which is due to the small cross section of the background and reasonable selection efficiencies, reveals that the signal can be observed earlier before the scaled integrated luminosity of 500 fb^{-1} is achieved.

For comparison, the current results lead to 1015 signal

$\sqrt{s} = 500$ GeV, int. lumi = 500 fb^{-1}				
Background processes				
	ZZ	$t\bar{t}$	WW	Z/γ
ϵ_B	7×10^{-6}	$< 10^{-7}$	$< 10^{-7}$	$< 10^{-7}$
Signal processes				
	BP1	BP2	BP3	BP4
ϵ_S	0.077	0.076	0.076	0.064
S	1015	670	381	109
B	2			
S/B	482	318	180	47
S/\sqrt{B}	700	462	262	72
S'	103	80	57	25

Table VI. Signal and Background selection efficiencies and the signal significance in different benchmark points at $\sqrt{s} = 500$ GeV. The second significance estimator S' is defined as $S' = \sqrt{2((S+B)\ln(1+S/B) - S)}$ ([32, 43]). Background efficiencies have been obtained from a sample of 10M events and no event of $t\bar{t}$, WW or Z/γ remains.

$\sqrt{s} = 1000$ GeV, int. lumi = 500 fb^{-1}						
Background processes						
	ZZ	$t\bar{t}$	WW	Z/γ		
ϵ_B	4×10^{-6}	$< 10^{-7}$	$< 10^{-7}$	$< 10^{-7}$		
Signal processes						
	BP1	BP2	BP3	BP4	BP5	BP6
ϵ_S	0.053	0.066	0.07	0.073	0.075	0.076
S	328	342	322	304	272	241
B	0.2					
S/B	652	680	641	605	540	480
S/\sqrt{B}	462	482	455	428	383	340
S'	60	61	59	57	54	50

Table VII. Signal and Background selection efficiencies and the signal significance in different benchmark points at $\sqrt{s} = 1000$ GeV. S' is defined as mentioned in the caption of Tab. VI.

and 2 background events at 500 fb^{-1} for the first benchmark point which is $m_H = m_A = 150$ GeV and is the closest to the point chosen by [32]. This means that at 100 fb^{-1} one would have 203 signal vs 0.4 background events which is consistent with their results.

Figures 5 and 6 show the signal on top of the background. The size of the MC sample used to obtain these

plots is two orders of magnitude larger than the actual size of the expected sample from the real experiment. However the final results have been scaled to the integrated luminosity of 500 fb^{-1} . The detector effects have been propagated into the final results in terms of momentum and energy smearing. As seen from these figures, the signal is well visible in a clean environment with small background contamination. The signal with $m_H = 200 \text{ GeV}$ and $m_A = 250 \text{ GeV}$ has a small cross section at $\sqrt{s} = 500 \text{ GeV}$ but is still observable. The analysis at $\sqrt{s} = 1 \text{ TeV}$ is effectively a background free analysis with a very tiny background at the Z mass. Signal of the first benchmark point is expected to be visible at even lower center of mass energy corresponding to the ILC operation at $\sqrt{s} = 350 \text{ GeV}$. This expectation can be verified in detail but what was shown in this analysis is the dramatic potential of linear colliders for the 2HDM Higgs boson observation at moderate masses even though at a specific model type.

V. CONCLUSIONS

Signals of the 2HDM Higgs bosons were analyzed for the case of unpolarized e^+e^- collisions at $\sqrt{s} = 500$ and 1000 GeV . Different benchmark points were studied for the two operation scenarios. Assuming 2HDM type IV as the theoretical framework, the Higgs bosons decay to $\tau\tau$ was analyzed focusing on the hadronic τ decays. The detector simulation was performed based on parameters from the SiD detector studies at ILC. Results can be summarized as follows.

The Higgs boson decay to $\tau\tau$ is dominant as long as decays to gauge bosons are kinematically forbidden. The decay to $\tau\tau$ reaches $\sim 80\%$ at $\tan\beta = 3$ for both H and A . The signal has a small sensitivity to the value of $\tan\beta$ and results are valid for $\tan\beta > 3$ with neg-

ligible variation. There is also negligible sensitivity of $\text{BR}(H/A \rightarrow \tau\tau)$ to the Higgs bosons masses as long as $m_A - m_H < m_Z$. The signal rate thus depends only on phase space (Higgs bosons masses) and tends to decrease when $m_H + m_A$ reaches the collider center of mass energy. This can be seen by following results of the analyses of the chosen benchmark points. However, due to the reasonable performance of kinematic algorithm used in the analysis, striking signals are observable at high statistical significances even when $m_H + m_A$ is below \sqrt{s} by 50 GeV (BP4). The signal is thus expected to be observable for all m_H and m_A values as long as $m_H + m_A$ is less than \sqrt{s} . The conclusion does not depend sizably on the value of $\tan\beta$. The value of α should of course be extracted from $\sin(\beta - \alpha) = 1$ which is the SM-like assumption.

Results obtained in the current analysis are beyond the reach of LHC as their main search channel is through $A \rightarrow ZH$ decay which is suitable for $\tan\beta < 3$ and large mass splitting between H and A . At the ILC, The signals of the Higgs bosons are observable as sharp distributions on top of the background at integrated luminosity of 500 fb^{-1} and already much lower luminosities are sufficient for discovery. Therefore the signal cross section can be measured from data with a reasonable precision. Such precision measurements can be used to verify the model type (through Higgs boson coupling to leptons) and α and β angles through Higgs boson coupling to gauge bosons. Therefore it is expected that such a background free signal would serve as a tool to analyze the 2HDM parameter space.

ACKNOWLEDGMENTS

We would like to thank the college of sciences at Shiraz university for providing computational facilities during the research program.

-
- [1] S. Chatrchyan *et al.* (CMS), Phys. Lett. **B716**, 30 (2012), arXiv:1207.7235 [hep-ex].
 - [2] G. Aad *et al.* (ATLAS), Phys. Lett. **B716**, 1 (2012), arXiv:1207.7214 [hep-ex].
 - [3] F. Englert and R. Brout, Phys. Rev. Lett. **13**, 321 (1964).
 - [4] P. W. Higgs, Phys. Rev. Lett. **13**, 508 (1964).
 - [5] P. W. Higgs, Phys. Lett. **12**, 132 (1964).
 - [6] G. S. Guralnik, C. R. Hagen, and T. W. B. Kibble, Phys. Rev. Lett. **13**, 585 (1964).
 - [7] P. W. Higgs, Phys. Rev. **145**, 1156 (1966).
 - [8] T. W. B. Kibble, Phys. Rev. **155**, 1554 (1967).
 - [9] T. D. Lee, Phys. Rev. **D8**, 1226 (1973).
 - [10] S. L. Glashow and S. Weinberg, Phys. Rev. **D15**, 1958 (1977).
 - [11] G. C. Branco, Phys. Rev. **D22**, 2901 (1980).
 - [12] M. Hashemi and M. Mahdavihorrami, Eur. Phys. J. **C78**, 485 (2018), arXiv:1804.10790 [hep-ph].
 - [13] M. Hashemi and G. Haghighat, (2018), arXiv:1805.00686 [hep-ph].
 - [14] M. Hashemi, The European Physical Journal C **77**, 302 (2017).
 - [15] M. Hashemi and G. Haghighat, Physics Letters B **772**, 426 (2017).
 - [16] H. E. Haber and D. O'Neil, Phys. Rev. **D74**, 015018 (2006), [Erratum: Phys. Rev.D74,no.5,059905(2006)], arXiv:hep-ph/0602242 [hep-ph].
 - [17] G. C. Branco, P. M. Ferreira, L. Lavoura, M. N. Rebelo, M. Sher, and J. P. Silva, Phys. Rept. **516**, 1 (2012), arXiv:1106.0034 [hep-ph].
 - [18] J. Abdallah *et al.* (DELPHI), Eur. Phys. J. **C38**, 1 (2004), arXiv:hep-ex/0410017 [hep-ex].
 - [19] T. Aaltonen *et al.* (CDF), Phys. Rev. Lett. **103**, 201801 (2009), arXiv:0906.1014 [hep-ex].
 - [20] V. M. Abazov *et al.* (D0), Phys. Rev. Lett. **107**, 121801 (2011), arXiv:1106.4885 [hep-ex].
 - [21] V. M. Abazov *et al.* (D0), Phys. Lett. **B710**, 569 (2012), arXiv:1112.5431 [hep-ex].

- [22] V. Khachatryan *et al.* (CMS), Phys. Lett. **B748**, 221 (2015), arXiv:1504.04710 [hep-ex].
- [23] G. Aad *et al.* (ATLAS), Phys. Lett. **B744**, 163 (2015), arXiv:1502.04478 [hep-ex].
- [24] M. Aaboud *et al.* (ATLAS), Phys. Lett. **B783**, 392 (2018), arXiv:1804.01126 [hep-ex].
- [25] H. Abramowicz *et al.*, (2013), arXiv:1306.6329 [physics.ins-det].
- [26] T. Barklow, J. Brau, K. Fujii, J. Gao, J. List, N. Walker, and K. Yokoya, (2015), arXiv:1506.07830 [hep-ex].
- [27] L. Linssen, A. Miyamoto, M. Stanitzki, and H. Weerts, (2012), 10.5170/CERN-2012-003, arXiv:1202.5940 [physics.ins-det].
- [28] M. Aicheler, M. Aicheler, P. Burrows, M. Draper, T. Garvey, P. Lebrun, K. Peach, N. Phinney, H. Schmickler, D. Schulte, *et al.*, (2012), 10.5170/CERN-2012-007.
- [29] P. Lebrun, L. Linssen, A. Lucaci-Timoce, D. Schulte, F. Simon, S. Stapnes, N. Toge, H. Weerts, and J. Wells, (2012), 10.5170/CERN-2012-005, arXiv:1209.2543 [physics.ins-det].
- [30] H. Abramowicz *et al.*, Eur. Phys. J. **C77**, 475 (2017), arXiv:1608.07538 [hep-ex].
- [31] S. Kanemura, K. Tsumura, and H. Yokoya, Phys. Rev. **D85**, 095001 (2012), arXiv:1111.6089 [hep-ph].
- [32] S. Kanemura, K. Tsumura, and H. Yokoya, in *International Workshop on Future Linear Colliders (LCWS11) Granada, Spain, September 26-30, 2011* (2012) arXiv:1201.6489 [hep-ph].
- [33] S. Schael *et al.* (DELPHI, OPAL, ALEPH, LEP Working Group for Higgs Boson Searches, L3), Eur. Phys. J. **C47**, 547 (2006), arXiv:hep-ex/0602042 [hep-ex].
- [34] M. Misiak *et al.*, Phys. Rev. Lett. **114**, 221801 (2015), arXiv:1503.01789 [hep-ph].
- [35] M. Misiak and M. Steinhauser, The European Physical Journal C **77**, 201 (2017).
- [36] A. Arbey, F. Mahmoudi, O. Stal, and T. Stefaniak, (2017), arXiv:1706.07414 [hep-ph].
- [37] S. Davidson and H. E. Haber, Phys. Rev. **D72**, 035004 (2005), [Erratum: Phys. Rev.D72,099902(2005)], arXiv:hep-ph/0504050 [hep-ph].
- [38] V. D. Barger, J. L. Hewett, and R. J. N. Phillips, Phys. Rev. **D41**, 3421 (1990).
- [39] M. Aoki, S. Kanemura, K. Tsumura, and K. Yagyu, Phys. Rev. **D80**, 015017 (2009), arXiv:0902.4665 [hep-ph].
- [40] M. Aoki, S. Kanemura, K. Tsumura, and K. Yagyu, Phys. Rev. D **80**, 015017 (2009).
- [41] V. Khachatryan *et al.* (CMS), Phys. Lett. **B755**, 217 (2016), arXiv:1510.01181 [hep-ex].
- [42] G. Aad *et al.* (ATLAS), Eur. Phys. J. **C76**, 45 (2016), arXiv:1507.05930 [hep-ex].
- [43] S. Kanemura, K. Tsumura, K. Yagyu, and H. Yokoya, Phys. Rev. **D90**, 075001 (2014), arXiv:1406.3294 [hep-ph].
- [44] D. Eriksson, J. Rathsmann, and O. Stal, Comput. Phys. Commun. **181**, 189 (2010), arXiv:0902.0851 [hep-ph].
- [45] D. Eriksson, J. Rathsmann, and O. Stal, Comput. Phys. Commun. **181**, 833 (2010).
- [46] P. Bechtel, O. Brein, S. Heinemeyer, O. Stål, T. Stefaniak, G. Weiglein, and K. E. Williams, Eur. Phys. J. **C74**, 2693 (2014), arXiv:1311.0055 [hep-ph].
- [47] P. Bechtel, S. Heinemeyer, O. Stål, T. Stefaniak, and G. Weiglein, Eur. Phys. J. **C74**, 2711 (2014), arXiv:1305.1933 [hep-ph].
- [48] P. Z. Skands *et al.*, JHEP **07**, 036 (2004), arXiv:hep-ph/0311123 [hep-ph].
- [49] B. C. Allanach *et al.*, Comput. Phys. Commun. **180**, 8 (2009), arXiv:0801.0045 [hep-ph].
- [50] T. Sjostrand, S. Mrenna, and P. Z. Skands, Comput. Phys. Commun. **178**, 852 (2008), arXiv:0710.3820 [hep-ph].
- [51] T. Sjöstrand, S. Ask, J. R. Christiansen, R. Corke, N. Desai, P. Ilten, S. Mrenna, S. Prestel, C. O. Rasmussen, and P. Z. Skands, Comput. Phys. Commun. **191**, 159 (2015), arXiv:1410.3012 [hep-ph].
- [52] E. Boos, V. Bunichev, M. Dubinin, L. Dudko, V. Ilyin, A. Kryukov, V. Edneral, V. Savrin, A. Semenov, and A. Sherstnev (CompHEP), *Advanced computing and analysis techniques in physics research. Proceedings, 9th International Workshop, ACAT'03, Tsukuba, Japan, December 1-5, 2003*, Nucl. Instrum. Meth. **A534**, 250 (2004), arXiv:hep-ph/0403113 [hep-ph].
- [53] A. Pukhov, E. Boos, M. Dubinin, V. Edneral, V. Ilyin, D. Kovalenko, A. Kryukov, V. Savrin, S. Shichanin, and A. Semenov, (1999), arXiv:hep-ph/9908288 [hep-ph].
- [54] C. Adolphsen, M. Barone, B. Barish, K. Buesser, P. Burrows, J. Carwardine, J. Clark, H. Mainaud Durand, G. Dugan, E. Elsen, *et al.*, (2013), arXiv:1306.6328 [physics.acc-ph].
- [55] E. A. Kuraev and V. S. Fadin, Sov. J. Nucl. Phys. **41**, 466 (1985), [Yad. Fiz.41,733(1985)].
- [56] S. Jadach and B. F. L. Ward, Comput. Phys. Commun. **56**, 351 (1990).
- [57] M. Skrzypek and S. Jadach, Z. Phys. **C49**, 577 (1991).
- [58] P. Chen, Phys. Rev. **D46**, 1186 (1992).
- [59] S. Lukic (FCAL), in *Proceedings, 12th International School-Seminar on The Actual Problems of Microworld Physics. Vol.1: Gomel, Belarus, July 22 - September 28, 2013*, Vol. 1, JINR (JINR, Dubna, Russia, 2015) pp. 54–68.
- [60] G. Aarons *et al.* (ILC), (2007), arXiv:0709.1893 [hep-ph].
- [61] J. Alwall *et al.*, *Monte Carlos for the LHC: A Workshop on the Tools for LHC Event Simulation (MC4LHC) Geneva, Switzerland, July 17-16, 2006*, Comput. Phys. Commun. **176**, 300 (2007), arXiv:hep-ph/0609017 [hep-ph].
- [62] J. de Favereau, C. Delaere, P. Demin, A. Giammanco, V. Lemaitre, A. Mertens, and M. Selvaggi (DELPHES 3), JHEP **02**, 057 (2014), arXiv:1307.6346 [hep-ex].
- [63] C. T. Potter, in *Proceedings, International Workshop on Future Linear Colliders (LCWS15): Whistler, B.C., Canada, November 02-06, 2015* (2016) arXiv:1602.07748 [hep-ph].
- [64] M. Cacciari, in *Deep inelastic scattering. Proceedings, 14th International Workshop, DIS 2006, Tsukuba, Japan, April 20-24, 2006* (2006) pp. 487–490, [125(2006)], arXiv:hep-ph/0607071 [hep-ph].
- [65] M. Cacciari, G. P. Salam, and G. Soyez, Eur. Phys. J. **C72**, 1896 (2012), arXiv:1111.6097 [hep-ph].
- [66] W. Grimus, L. Lavoura, O. M. Ogreid, and P. Osland, J. Phys. **G35**, 075001 (2008), arXiv:0711.4022 [hep-ph].
- [67] R. Brun and F. Rademakers, *New computing techniques in physics research V. Proceedings, 5th International Workshop, AIHENP '96, Lausanne, Switzerland, September 2-6, 1996*, Nucl. Instrum. Meth. **A389**, 81 (1997).

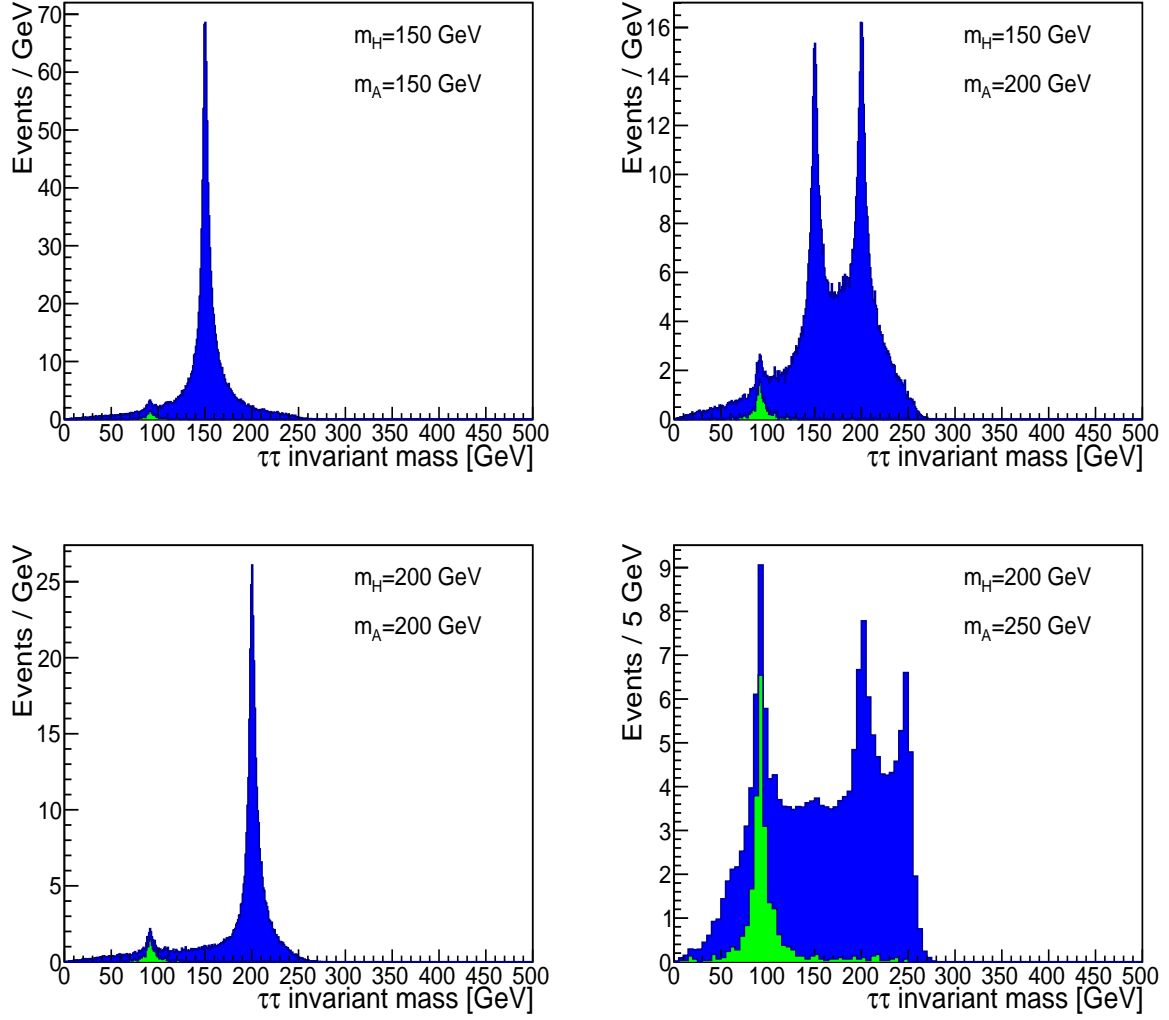


Figure 5. Signal of the τ -jet pair invariant mass in different benchmark points at $\sqrt{s} = 500$ GeV

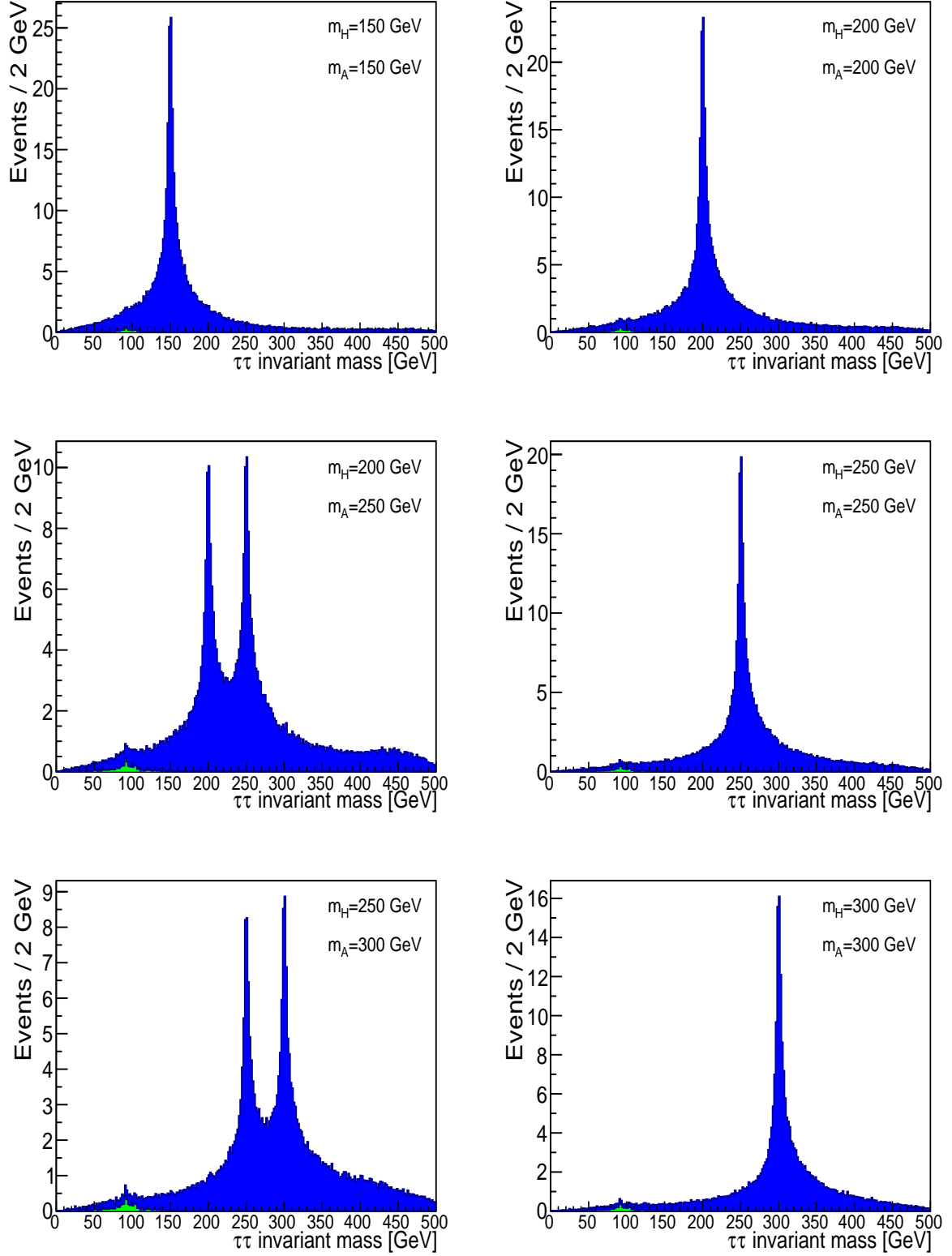


Figure 6. Signal of the τ -jet pair invariant mass in different benchmark points at $\sqrt{s} = 1000$ GeV